Mineralogical Magazine, December 2008, Vol. 72(6), pp. 1307–1318

Omongwaite, $Na_2Ca_5(SO_4)_6.3H_2O$, a new mineral from recent salt lake deposits, Namibia

F. MEES[1,*], F. HATERT[2] AND R. ROWE[3]

[1] Department of Geology and Mineralogy, Royal Museum for Central Africa, Leuvensesteenweg 13, B-3080 Tervuren, Belgium
[2] Laboratory of Mineralogy, Department of Geology, University of Liège, Building B-18, B-4000 Liège, Belgium
[3] Earth Sciences Section, Canadian Museum of Nature, PO Box 3443, Station D, Ottawa, Ontario K1P 6P4, Canada

[*Received 20 October 2008; Accepted 9 February 2009*]

ABSTRACT

Omongwaite, $Na_2Ca_5(SO_4)_6.3H_2O$, is a new mineral, found as inclusions in gypsum crystals in recent salt lake deposits at Omongwa pan, Namibia. It is monoclinic, with space group *C*2, *a* = 12.08(3) Å, *b* = 6.96(1) Å, *c* = 6.39(2) Å, ß = 90.2(3)º, *V* = 537(2) Å^3, and *Z* = 1. The six strongest lines in the X-ray powder diffraction pattern [$d_{obs.}$ (Å), ($I/I_{o\ meas.}$), (*hkl*)] are: 6.028, (40), (110); 3.484, (29), (310); 3.019, (51), (400); 3.014, (100), (220); 2.824, (34), (112); and 2.820, (65), ($\bar{1}12$). Electron microprobe analysis, recalculated on the basis of $3H_2O$ per formula unit (p.f.u.), gave 56.16 wt.% SO_3, 30.82 wt.% CaO, 5.25 wt.% Na_2O, 3.21 wt.% K_2O, 6.25 wt.% H_2O, totalling 101.69 wt.%. The empirical formula, based on 24 anhydrous oxygens p.f.u., is $(Na_{1.47}K_{0.59})_{\Sigma=2.06}Ca_{4.76}S_{6.07}O_{24}.3H_2O$, yielding $Na_2Ca_5(SO_4)_6.3H_2O$ as the end-member formula. Na/K ratios are variable, with an average of ~2.5. The crystals are elongated, with pseudohexagonal transversal cross-sections and with sphenoidal terminations that are commonly developed at one end. The crystal structure of omongwaite is similar to that of bassanite, $CaSO_4.0.5H_2O$. Published studies of the synthetic phase show that it can be described as a bassanite structure in which one out of six Ca^{2+} ions are replaced by Na^+ and a second Na^+ ion occupies a position near those sites. The crystals are parallel to the [001] axis of the gypsum crystals in which they occur as inclusions. The mineral formed by topotactic replacement during interaction of gypsum with concentrated solutions. It is preserved where the affected surface became covered by gypsum by rapid growth shortly after the formation of omongwaite. The mineral is named after the locality where it was found.

KEYWORDS: omongwaite, bassanite, new mineral, Omongwa pan, Namibia.

Introduction

THE Omongwa pan is a dry lake basin of the southwestern Kalahari. The pan deposits are lacustrine sediments that have been affected by extensive diagenetic gypsum formation in the upper part (Mees, 1999). The gypsum crystals commonly contain small mineral inclusions, identified as omongwaite, $Na_2Ca_5(SO_4)_6.3H_2O$, a new mineral. This mineral represents a natural occurrence of a compound that has been produced in laboratory conditions by several authors (Hill and Wills, 1938; Autenrieth, 1958; Autenrieth and Braune, 1959; Lepeshkov and Fradkina, 1959; Rassonskaya and Semendyaeva, 1961; Gudowius and Von Hodenberg, 1979; Rogozovskaya *et al.*, 1980; Rogozovskaya and Kononchuk, 1981; Reisdorf and Abriel, 1987; Freyer *et al.*, 1999, 2002). The mineral and name have been approved by the IMA Commission on New Minerals, Nomenclature and Classification (2003-054b). The mineral is named after the locality where it was found, 'omongwa' meaning 'salt' in the local language (Otjiherero) (Viljoen and Kamupingene,

* E-mail: florias.mees@africamuseum.be
DOI: 10.1180/minmag.2008.072.6.1307

1983). Holotype material is deposited at the Royal Museum for Central Africa, Tervuren, Belgium, under catalogue number RGM 15.908.

Occurrence and associated minerals

The mineral has been found in deposits of the Omongwa pan, near Aminuis, 140 km SSE of Gobabis, southwestern Kalahari, Namibia (23º41'S, 19º23'E). The upper lithological unit of the pan deposits (0–40/55 cm depth) is typically highly gypsiferous. Gypsum mainly occurs as lenticular crystals, formed by evaporation of groundwater. Subordinate occurrences of tabular gypsum crystals in voids, and of prismatic crystals in a thin surface layer, formed by subaqueous crystallization after flooding (Mees, 1999). In part of the basin, the deposits contain kalistrontite, $K_2Sr(SO_4)_2$, the formation of which is related to groundwater evaporation. Minor amounts of syngenite, $K_2Ca(SO_4)_2.2H_2O$, occur in the uppermost part of the profiles (mainly <0.5 cm depth). It occurs as coatings around gypsum crystals and is formed by an interaction with K-rich brines.

Omongwaite occurs as inclusions in gypsum crystals. It can be identified in most of the available samples of the gypsiferous upper part of the pan deposits, i.e. 33 out of the 36 samples from this interval that were used in an earlier study (Mees, 1999). Inclusions are present in greater relative numbers of gypsum crystals in higher parts of the unit. The gypsum crystals contain greater concentrations of inclusions in those parts. The few samples in which inclusions are absent, represent the lowest gypsum-bearing part of the section. Inclusions occur in lenticular crystals in the subsurface horizons and in prismatic crystals of the surface deposits, but they are absent in tabular crystals within voids.

Physical properties

Omongwaite crystals can range up to 200 μm in length and 20 μm in width but usually are much smaller. They have an elongated habit, generally with a sphenoidal termination developed at one end (Fig. 1*a*). Typically, transverse sections display a pseudohexagonal form (Fig. 1*b*).

Macroscopic data and density measurements are impossible to obtain, due to the small size of the crystals and the nature of their occurrence. The crystals are only observed in thin sections and cannot be isolated from the enclosing gypsum. Using the chemical composition represented by the empirical formula, the calculated density = 2.720 g/cm^3.

In thin section, omongwaite is transparent, colourless and non-fluorescent, and shows no cleavage. The refractive indices are greater than those of gypsum for all orientations, i.e. >1.53 ($n_{calc.}$ = 1.540). Birefringence is ~0.015, based on the highest interference colours of large crystals. The orientation is Z ~ *c*, and extinction is slightly oblique (<10º). The axial figure could not be determined. Optical properties reported for synthetic $Na_2Ca_5(SO_4)_6.3H_2O$ are n_α = 1.5557, n_γ = 1.567, and Z^*c* = 11º (Hill and Wills, 1938; Rassonskaya and Semendyaeva, 1961). For synthetic $(Na,K)_2Ca_5(SO_4)_6.3H_2O$, the $2V_{meas.}$

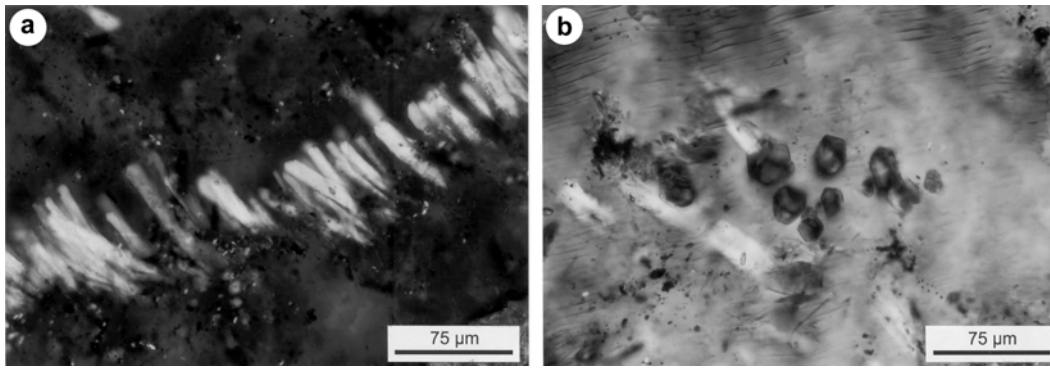

FIG. 1. (*a*) Omongwaite inclusions in a gypsum crystal, consisting of elongated prismatic crystals with sphenoidal terminations at one end (site 36, 7–16 cm, cross-polarized light (XPL)) (for site locations, see Mees, 1999); (*b*) mainly transverse cross-sections of omongwaite crystals, showing a pseudohexagonal form (site 30, 4–23 cm, XPL).

TABLE 1. Chemical composition, determined by WDS analysis at −192ºC (average of 175 analyses).

	Wt.%	Range	Std. dev.	Standard
SO_3	56.16	51.49−59.65	1.27	Baryte
CaO	30.82	29.12−33.36	0.65	Andradite
Na_2O	5.25	4.14−6.26	0.39	Albite
K_2O	3.21	2.46−4.40	0.41	Sanidine
H_2O*	6.25			
Total	101.69			

* calculated.

was determined to be smaller than 20º (Gudowius and Von Hodenberg, 1979).

Chemical composition

The chemical composition of omongwaite was determined by wavelength dispersive microanalysis of omongwaite in polished thin sections. This was carried out with a Cameca Camebax Micro system at the Department of Earth Sciences, University of Bristol, UK. This instrument was equipped with a cold stage which permits cooling of the specimen to a temperature of −192ºC which was required to limit dehydration and alkali cation migration within the specimen. Stable count rates were maintained at −192ºC for a 5 μm spot size when the system was operated using a 15 kV accelerating potential, 5 nA probe current and 10 s count times. The inclusions are easily recognized in backscattered electron mode as areas with much lighter grey values than gypsum. Matrix corrections were applied using the PAP correction procedure of Pouchou and Pichoir (1988).

The mean analytical results, derived from a total of 175 analyses, are reported in Table 1. The instability of the mineral under the electron beam, revealed by the appearance of burn marks, results in higher oxide contents and a H_2O content that is too low if calculated by assigning the deficit in the total of the weight percentages of the oxides to water, corresponding to $2.19H_2O$ p.f.u. H_2O was therefore calculated on the basis of $3H_2O$ p.f.u., based on the stoichiometry of the synthetic phase. The empirical formula, based on 24 anhydrous oxygen atoms p.f.u., is $(Na_{1.47}K_{0.59})_{\Sigma=2.06}Ca_{4.76}S_{6.07}O_{24}.3H_2O$. The end-member formula is $Na_2Ca_5(SO_4)_6.3H_2O$, which requires 7.07 wt.% Na_2O, 31.98 wt.% CaO, 54.78 wt.% SO_3 and 6.17 wt.% H_2O to satisfy the stoichiometry. The Na/K ratio is between 2.05 and 3.08, with an average of 2.48.

TABLE 2. Raman spectrum of omongwaite, compared to those of bassanite and gypsum.

— Omongwaite[1] —		— Bassanite[2] —		— Gypsum[3] —	
cm^{-1}	band	cm^{-1}	band	cm^{-1}	band
436	ν_2SO_4	434	ν_2SO_4	416	ν_2SO_4
476	ν_2SO_4	488	ν_2SO_4	495	ν_2SO_4
–	–	–	–	582	ν_TH_2O
608	ν_4SO_4	–	–	605	ν_4SO_4
–	–	–	–	620	ν_4SO_4
637	ν_4SO_4	630	ν_4SO_4	625	ν_4SO_4
665	ν_4SO_4	672	ν_4SO_4	673	ν_4SO_4
1013	ν_1SO_4	1017	ν_1SO_4	1008	ν_1SO_4
–	–	1124	ν_3SO_4	1119	ν_3SO_4
1143	ν_3SO_4	1154	ν_3SO_4	1135	ν_3SO_4
–	–	1168	ν_3SO_4	1140	ν_3SO_4
–	–	–	–	1631	ν_2H_2O
–	–	–	–	1678	ν_2H_2O
–	–	3516	H_2O	3405	ν_1H_2O
3527	ν_2O	3568	H_2O	3491	ν_3H_2O

[1] This study.
[2] Chang *et al*. (1999).
[3] Kloprogge and Frost (2000), assignments as in Hass and Sutherland (1956).

The presence of water groups is confirmed by the recognition of a νH_2O band around 3530–3540 cm^{-1} in Raman spectra (Senterra Raman microscope, Koninklijk Belgisch Instituut voor Natuurwetenschappen, Brussels) (Table 2; Fig. 2). As expected, the ν_2H_2O band around 1630 cm^{-1}, recognized in infrared absorption spectra for gypsum ($CaSO_4.2H_2O$) and bassanite ($CaSO_4.0.5H_2O$) (e.g. Bensted and Prakash, 1968; Putnis *et al.*, 1990), is absent, but this band is also lacking in spectra recorded for the enclosing gypsum during the same session. The ν_2H_2O band is in fact absent in several published Raman spectra for gypsum (e.g. Dickinson and Dillon, 1929; Sarma *et al.*, 1998; Chang *et al.*, 1999), and has never been reported for bassanite in Raman studies. The spectra for omongwaite show several vibrational bands attributed to sulphate groups, according to the assignments proposed for bassanite and gypsum (Table 2). The strong absorption band at 1012 to 1015 cm^{-1} (ν_1SO_4) is characteristic of omongwaite and permits its distinction from the enclosing gypsum (1007–1008 cm^{-1}). The wavenumber value of this band is similar to that of its equivalent in bassanite spectra. Reported values for the ν_1SO_4 mode of bassanite and gypsum show some variation but they are consistently higher for bassanite (e.g. Bensted and Prakash, 1968; Sarma *et al.*, 1998; Chang *et al.*, 1999; Prasad, 1999; Chio *et al.*, 2004; Prasad *et al.*, 2005), a systematic difference with gypsum that is also observed in omongwaite. Prasad *et al.* (1998) report minor shifts related to the nature of cations

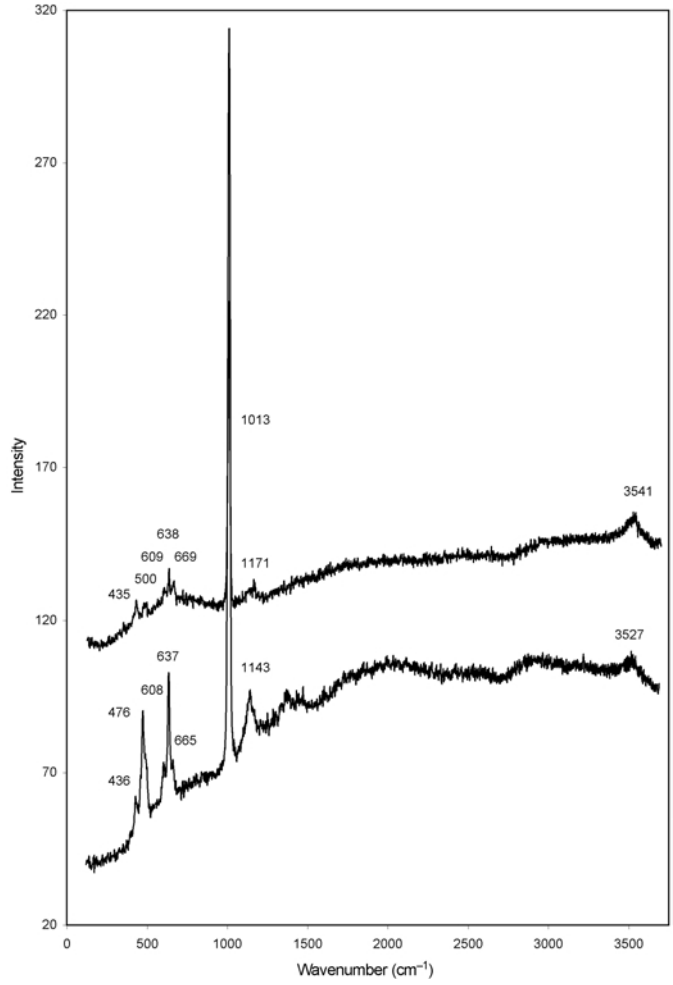

FIG. 2. Raman spectra of omongwaite.

occurring as impurities in bassanite. Published Raman data for synthetic $Na_2Ca_5(SO_4)_6.3H_2O$ are limited to the ν_4SO_4 mode (Freyer *et al.*, 2002), showing the same type of deviation from bassanite spectra as is recorded for omongwaite (see Table 2).

X-ray diffraction analysis

X-ray powder-diffraction data for a single crystal (Table 3) were collected with a Bruker AXS Discover 8 microdiffractometer using a Hi-Star 2-D area detector operated with a GADDS system, Cu-$K\alpha_1$ radiation at 40 kV/40 mA and with a sample-to-detector distance of 12 cm. The instrument was calibrated with synthetic corundum. Data were collected from a 100 μm crystal, cut from a thin section and analysed using a pseudo-Gandolfi approach, in which the crystal lies at the end of a mount on a fixed-Chi stage (54.736º) and is slowly rotated 360º around one axis while the data are being collected. This crystal was too small to permit the use of conventional X-ray powder diffraction methods.

The diffraction pattern gives reliable peak positions but unreliable intensities. However,

TABLE 3. X-ray powder-diffraction data for omongwaite.

Omongwaite (pure) [GADDS]		Omongwaite (in mixture with gypsum)* [Gandolfi]		Omongwaite (calculated)**			Synthetic $Na_2Ca_5(SO_4)_6.3H_2O$ (PDF 89-8618; Freyer *et al.*, 1999)			Synthetic $Na_2Ca_5(SO_4)_6.3H_2O$ (calculated using ICSD structure data)***		
$d_{obs.}$	$I/I_{o\ meas.}$	$d_{obs.}$	$I/I_{o\ meas.}$	$d_{obs.}$	$I/I_{o\ meas.}$	*hkl*	$d_{obs.}$	$I/I_{o\ meas.}$	*hkl*	$d_{calc.}$	$I/I_{o\ calc.}$	*hkl*
				6.037	21	200	6.045	60	200	6.045	21	200
6.005	–	6.053	75	6.028	40	110	5.995	78	110	5.995	40	110
							4.383	*5*	*$\bar{2}$01*			
							4.359	*8*	*$\bar{1}$11*			
3.481	–	3.503	50	3.484	29	310	3.480	33	310	3.480	29	310
				3.478	14	020	3.452	20	020	3.452	14	020
							3.054	*11*	*$\bar{3}$11*	*3.054*	*11*	*$\bar{3}$11*
										3.051	*6*	*311*
				3.019	51	400	3.022	42	400	3.022	51	400
3.015	–	3.038	100	3.014	100	220	2.997	78	220	2.997	100	220
				2.828	12	202	2.808	100	202	2.814	12	$\bar{2}$02
				2.824	34	112				2.810	34	202
2.819	–	2.815	100	2.820	65	$\bar{1}$12				2.805	65	$\bar{1}$12
				2.818	22	$\bar{2}$02				2.806	22	112
							2.728	*5*	*$\bar{4}$01*			
							2.712	*8*	*$\bar{2}$21*	*2.712*	*11*	*$\bar{2}$21*
							2.348	*5*	*$\bar{3}$12*			
							2.345	*5*	*312*			
							2.337	*5*	*022*			
				2.151	8	511	2.147	5	$\bar{5}$11	2.146	8	511
2.139	–	2.146	<25	2.145	10	$\bar{4}$21	2.142	8	$\bar{4}$21	2.142	10	$\bar{4}$21
				2.144	8	$\bar{1}$31	2.130	5	$\bar{1}$31	2.130	8	$\bar{1}$31
				2.129	15	003	2.118	8	003	2.118	15	003
							1.906	*5*	*$\bar{3}$31*	*1.9057*	*7*	*331*
1.8534	–	–	–	1.8529	23	$\bar{5}$12	1.855	18	$\bar{5}$12	1.8546	23	$\bar{5}$12
				1.8584	23	422	1.848	22	$\bar{4}$22	1.8579	23	422
				1.8548	24	132	1.842	21	$\bar{1}$32	1.8515	24	132
1.7437	–	–	–	1.7419	7	620	1.740	5	620	1.7400	7	620
				1.7059	10	602	1.700	7	$\bar{6}$02	1.7003	10	602
1.7011	–	–	–	1.6990	18	$\bar{3}$32	1.692	13	$\bar{3}$32	1.6920	18	$\bar{3}$32

* *d* values for gypsum not included

** *d* values calculated from XRPD cell refinement with a = 12.08(3), b = 6.96(1), c = 6.39(2) Å, β = 90.2(3)º, V = 537(2) Å^3; intensities as for calculated pattern using synthetic $Na_2Ca_5(SO_4)_6.3H_2O$ atom coordinates (ICSD # 88943)

*** Calculated using synthetic $Na_2Ca_5(SO_4)_6.3H_2O$ atom coordinates from ICSD # 88943 (*ATOMS* v. 6.0).

Italicized values indicate peaks which do not appear in the omongwaite (calculated) pattern (columns 5–7).

measured intensity values are available from a powder-diffraction pattern recorded for a fragment of gypsum enclosing an omongwaite crystal which could not be separated from the gypsum host (Gandolfi camera, Fe-*K*α radiation) (Table 3).

Indexing of the measured patterns was achieved by comparing the intensities with those from a pattern for synthetic $Na_2Ca_5(SO_4)_6.3H_2O$ that was calculated using atom coordinates from the Inorganic Crystal Structure Database (ICSD) (*ATOMS* v. 6.0 software), as determined by Freyer *et al.* (1999) for the synthetic analogue (Table 3).

The derived unit-cell parameters, refined using the *CELREF* program, are a = 12.08(3) Å, b = 6.96(1) Å, c = 6.39(2) Å, β = 90.2(3)º, V = 537(2) Å^3 and Z = 1. The mineral is monoclinic, space group *C*2. The lattice parameters and other physical properties of omongwaite, the synthetic analogue and bassanite are listed in Table 4.

Structure refinement for synthetic $Na_2Ca_5(SO_4)_6.3H_2O$, based on single-crystal data, show that its crystal structure is similar to that of bassanite (Freyer *et al.*, 1999). Unit-cell parameters reported by those authors are a = 12.0890(11) Å, b = 6.903(2) Å, c = 6.3537(12), Å, β = 90.089(2), V = 530.2(2) Å^3 and Z = 1. In comparison with the structure of bassanite, one out of six Ca^{2+} is are replaced by Na^+, and a second Na^+ ion occupies a position near those sites, resulting in charge compensation. This replacement brings about a distortion of the bassanite lattice, resulting in a superstructure with doubled a, b and c lattice constants. The number of Ca^{2+} ions that can be replaced is limited because it is restricted to half of the Ca^{2+} ions with a specific co-ordination (Freyer *et al.*, 1999). The resulting structure comprises alternating planes of $CaSO_4$ groups and planes with parallel strings of $CaSO_4$-$NaSO_4$ groups and H_2O- and Na^+-containing channels, parallel to the c axis (Freyer *et al.*, 1999). In synthetic $(Na,K)_2Ca_5(SO_4)_6.3H_2O$, the occurrence of the larger K^+ ions, which are probably confined to the channel positions, results in slightly greater lattice constant values (Freyer *et al.*, 2002).

Arrangement and distribution within the gypsum crystals

The omongwaite inclusions mainly occur as bands or smaller groups of parallel crystals, with a constant orientation between these clusters throughout the gypsum host (Fig. 3*a*). The crystals are generally not perfectly aligned, showing small variations in orientation that produce fan-like or random patterns (Fig. 3*b*).

The bands of inclusions are parallel to the sides of the gypsum crystals, with an inward orientation of the euhedral terminations (see Fig. 3*a*). The base of the inclusions is never in contact with the side of the crystal. The gypsum that covers the level containing the inclusions generally has a higher sediment content than other parts of the same crystal (see Figs 3*b*, 4*c*). In several gypsum crystals, a band containing inclusions completely surrounds a large central zone with a low sediment content. These zones have a lenticular form in some crystals, but they are mainly

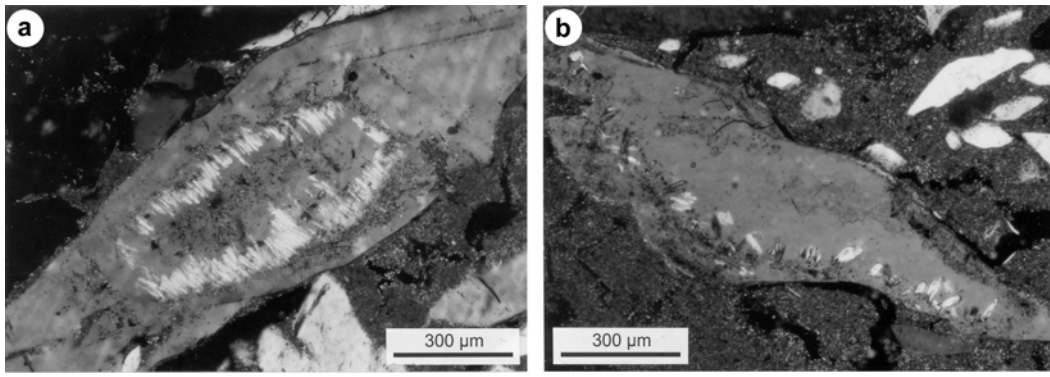

FIG. 3. (*a*) Parallel orientation of omongwaite crystals throughout a gypsum crystal (site 36, 7–16 cm, XPL); (*b*) Imperfect alignment of omongwaite crystal in a cross-section that is roughly parallel to the (010) orientation of the gypsum host (site 33, 47–55 cm, XPL).

TABLE 4. Comparison between the physical properties of omongwaite, its synthetic analogue, and bassanite.

	Omongwaite	Synthetic analogue	Bassanite
Unit-cell parameters	a = 12.08(3) Å b = 6.96(1) Å c = 6.39(2) Å β = 90.2(3)°	a = 12.089(1) Å b = 6.903(2) Å c = 6.354(1) Å β = 90.09(1)°[1]	a = 12.0340(6) Å b = 6.9284(6) Å c = 12.672(1) Å β = 90.265(3)°[7]
Space group	$C2$	$C2$[1]	$I2$[7]
X-ray data (d in Å, and I/I_0)	6.005(75), 3.481(50), 3.015(100), 2.819(100), 2.139(20), 1.8534(major), 1.7437(minor), 1.7011(minor)	6.045(60), 5.995(78), 3.480(33), 3.022(42), 2.997(78), 2.808(100), 1.848(22), 1.842(21)[2] 6.03(50), 3.82(15), 3.47(40), 3.01(100), 2.82(80), 2.13(15), 1.85(40), 1.70(30)[3]	6.012(90), 3.468(80), 3.004(90), 2.802(100), 2.137(50), 2.112(40), 1.851(60), 1.843(85)[8] 6.01(80), 3.47(50), 3.01(100), 2.80(90), 1.849(20), 1.845(30), 1.693(20), 1.665(20)[9]
Morphology	acicular, elongated along [001]; sphenoidal terminations at one end; pseudohexagonal transverse cross-sections	elongated along [001], flattened parallel to (010); presence of {110}, {001}, {101}, {102}; twinning along (101) or (10$\bar{1}$); pseudohexagonal transversal cross-sections[1,4]	elongated along [010], terminated by trigonal pyramids; twinning along (101)[8]
Density (g/cm^3)	$\rho_{calc.}$ = 2.720	$\rho_{calc.}$ = 2.734[1] $\rho_{meas.}$ = 2.72(2)[4]	ρ = 2.731[9]
Optical properties	n = 1.540 Δ ~ 0.015 Z^c < 10° colourless	α = 1.5557, γ = 1.567[5,6] Z^c = 11°[5] $2V_{meas.}$ < 20°[4]	α = 1.550, γ = 1.577[10] Z ~ c[10] small 2V[10]

[1] Freyer *et al*. (1999); [2] PDF 89-8618 (Freyer *et al.*, 1999); [3] Reisdorf and Abriel (1987); [4] Gudowius and Von Hodenberg (1979); [5] Hill and Wills (1938); [6] Rassonskaya and Semendyaeva (1961); [7] Ballirano *et al*. (2001); [8] Lager *et al*. (1984); [9] Gaines *et al*. (1997); [10] Allen and Kramer (1953).

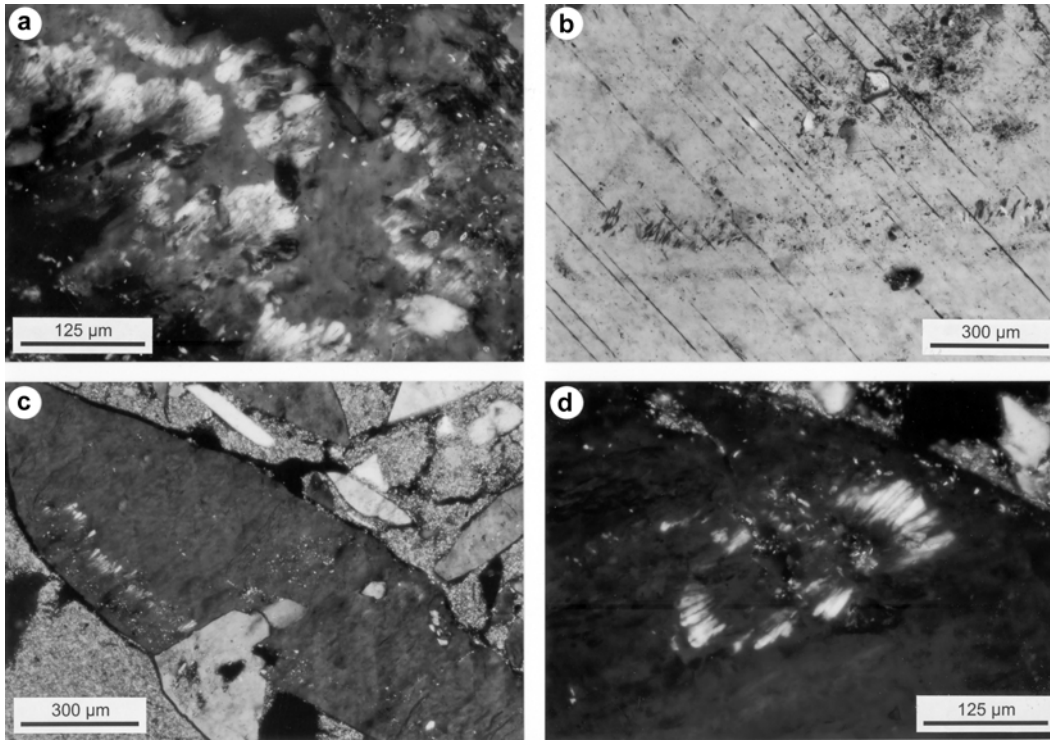

FIG. 4. (*a*) Omongwaite inclusions surrounding an anhedral central zone with a small sediment content of the gypsum host (site 4, 0−7 cm, XPL); (*b*) omongwaite crystals, mainly at or near extinction position, along a band with high sediment content in a gypsum crystal with zonation (site 33, 47−55 cm, XPL); (*c*) omongwaite crystals at a level that corresponds to the surface of the gypsum host in part of the crystal (site 4, 40−45 cm, XPL); (*d*) omongwaite inclusions surrounding a central zone with a greater sediment content, with an outward orientation of the euhedral terminations (site 2, 5−24 cm, XPL).

anhedral (Fig. 4*a*). Inclusions also occur along the inner side of thin bands that are part of the patterns of zonation (Fig. 4*b*). In one crystal, the base of a band of inclusions coincides with the lateral extension of the curved surface that forms the side of the crystal where no overgrowth developed (Fig. 4*c*). Along that side, the gypsum crystal only contains a few small inclusions, which appear to be remnants of longer crystals.

A less common type of occurrence is represented by bands with inclusions that partly, or completely, surround a central zone with a high sediment content (Fig. 4*d*). In these bands, the euhedral terminations of the omongwaite crystals point away from the surrounded area. An outward orientation also characterizes inclusions that occur along part of the sides of cavities (Fig. 5*a*). The base of these inclusions is generally not in contact with the side of the voids.

In some gypsum crystals containing a sediment-rich core and an outer part without sediment inclusions, the presence of omongwaite inclusions is strictly confined to the core, with no preferential distribution or orientation relative to the sides of that zone (Fig. 5*b*).

Orientation relative to crystallographic orientation of enclosing gypsum

In subhedral prismatic gypsum crystals occurring in the surface layer of the pan deposits, the longitudinal axes of the inclusions are parallel to the {120} faces of the gypsum crystals in cross-sections parallel to (010) (Fig. 5*c*).

In lenticular gypsum crystals, transverse cross-sections of the inclusions are recognized in sections parallel to the plane of flattening of the enclosing gypsum, which has indices between

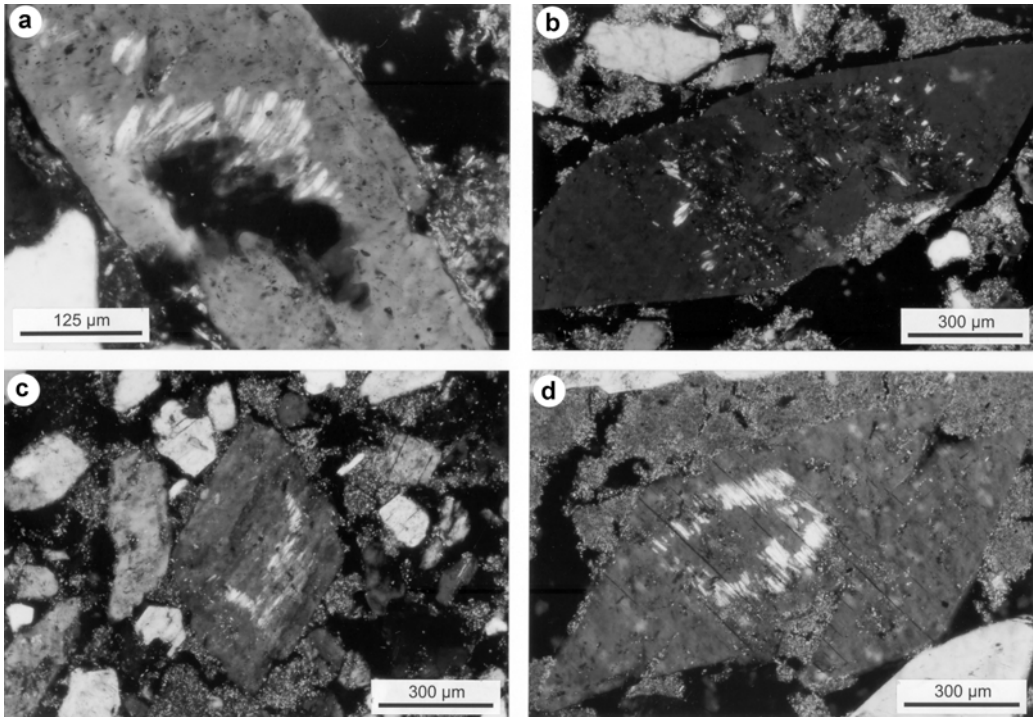

FIG. 5. (*a*) Omongwaite crystals along the sides of a cavity, with an outward orientation of the euhedral terminations (site 4, 30−40 cm, XPL); (*b*) Randomly oriented omongwaite crystals, throughout a sediment-rich part of a gypsum crystal (site 2, 5−24 cm, XPL); (*c*) Omongwaite inclusions in a subhedral prismatic gypsum crystal of a gypsum-rich surface layer, parallel to the {120} faces of the gypsum host (site 7, 0 cm, XPL); (*d*) Omongwaite inclusions parallel to the (010) cleavage planes of a lenticular gypsum crystal, in a cross-section perpendicular to (010) and at a large angle with the plane of flattening (site 36, 7−16 cm, XPL).

($\bar{1}01$) and ($\bar{1}03$). In cross-sections that are both at a large angle with the plane of flattening and perpendicular to (010), the longitudinal axes of the inclusions are well aligned and parallel to the (010) cleavage planes (Fig. 5*d*). In cross-sections parallel to (010), the longitudinal axes of the inclusions enclose a large angle with the longitudinal axis of the gypsum crystals (>45º) and an angle of 30−40º with the extinction position of the gypsum host.

These observations demonstrate that the preferential orientation of the longitudinal axis of the inclusions is parallel to the [001] axis of the gypsum crystal in which they occur. Their orientation varies to a greater extent within the (010) plane than in other directions (see Fig. 3*b*). Although this relationship characterizes most occurrences of the inclusions, different orientations are observed in a few cross-sections. These subordinate orientations are not clearly related to crystallographic orientations of the gypsum host.

Discussion

The nature of omongwaite

Synthetic $Na_2Ca_5(SO_4)_6.3H_2O$ has been produced by various authors (Hill and Wills, 1938; Lepeshkov and Fradkina, 1959; Rassonskaya and Semendyaeva, 1961; Rogozovskaya *et al.*, 1980; Rogozovskaya and Konochuk, 1981; Reisdorf and Abriel, 1987; Freyer *et al.*, 1999; Freyer *et al.*, 2002). A K-bearing variety was first described by Autenrieth (1958) and Autenrieth and Braune (1959), who reported a $(Na_{0.6},K_{0.4})_2Ca_5(SO_4)_6.3H_2O$ composition. A similar phase was obtained by Gudowius and Von Hodenberg (1979) $[(Na_{0.66},K_{0.375})_2Ca_{4.98}(SO_4)_6.3H_2O]$ and by Freyer *et al.* (2002) $[(Na_{0.55},K_{0.35})_2Ca_{4.98}(SO_4)_6.3H_2O]$. No other Na-K-Ca sulphates appear to have been reported for the Na_2SO_4-K_2SO_4-$CaSO_4$-H_2O system, which has not been the subject of later experiments or modelling (e.g. Harvie and Weare, 1980; Greenberg and Møller,

1989), in contrast to its anhydrous counterpart (Bellanca, 1942; Rowe *et al.*, 1972; Du, 2000).

Freyer *et al.* (1999) suggested that $Na_2Ca_5(SO_4)_6.3H_2O$ represents an end-member of a series with a continuous range of possible compositions between $Na_2Ca_5(SO_4)_6.3H_2O$ and bassanite – $Ca_6(SO_4)_6.3H_2O$. This is supported by reports of bassanite with intermediate Na concentrations. Concentrations of 0.50 wt.% Na_2O (Lager *et al.*, 1984), 3.01 wt.% Na_2O (Eipeltauer, 1956) and 4.04 wt.% Na_2O (Powell, 1962) have been measured for bassanite formed in saturated NaCl solutions. Kushnir (1982) reported bassanite compositions with high but variable Na/Ca and K/Ca ratios. An approximate $(Na,K)_2Ca_5(SO_4)_6.3H_2O$ stochiometry characterizes the samples with the highest Na+K content that he obtained, i.e. $(Na,K)_{1.96}Ca_{5.02}(SO_4)_6.3H_2O$ to $(Na,K)_{2.20}Ca_{4.90}(SO_4)_6.3H_2O$, with Na/K ratios of 1.48, 2.01 and 2.89 to 3.08 in different runs.

If a continuous range in composition exists between omongwaite and Na-free bassanite, all inclusions in gypsum crystals from the Omongwa pan formed under conditions in which the controlling physicochemical parameters had values that equalled or exceeded those that are required for the maximum possible degree of Ca^{2+} substitution. The measured Na/K ratios are rather variable and they are also different from those reported by others (Autenrieth, 1958; Autenrieth and Braune, 1959; Gudowius and Von Hodenberg, 1979). Experiments by Kushnir (1982) show that no correlation exists between Na/K ratios of the solid phase and those of the solution. Differences in ionic radius can be expected to limit the incorporation of K^+, or to restrict its occurrence to channel positions (Freyer *et al.*, 2002). However, the partition coefficients of K^+ are always greater than those of Na^+ for this crystal phase (Gudowius and Von Hodenberg, 1979; Kushnir, 1982).

Conditions of formation at the type locality

The phase boundaries for $Na_2Ca_5(SO_4)_6.3H_2O$ in the Na-Ca-SO_4-(Cl)-H_2O system were studied by Rogozovskaya *et al.* (1980) and Rogozovskaya and Kononchuk (1981). It is always metastable with respect to other phases (gypsum, anhydrite, thenardite, glauberite, eugsterite). It has been produced at temperatures of 25ºC and higher, with a decrease in the required Na concentration with increasing temperature.

In deposits of the Omongwa pan, omongwaite occurs as inclusions in gypsum crystals. It formed at the expense of gypsum by topotactic replacement. The preferential orientation of the longitudinal axes of the crystals coincides with the [001] axis of the gypsum crystals. Along that axis, Ca^{2+} and SO_4^{2-} ions are aligned in the gypsum crystal lattice (e.g. Weijnen *et al.*, 1987), suggesting a preservation of these strings in the omongwaite inclusions. This alignment is less perfect than in the case of transformation of gypsum to bassanite or anhydrite in the absence of a liquid phase, which is not unexpected when crystal growth is involved. The much stronger deviation from the [001] orientation within the (010) plane is also related to the crystal structure of gypsum, which is composed of alternating planes of Ca^{2+} and SO_4^{2-} ions and planes of H_2O molecules that are parallel to (010) (e.g. Heijnen and Hartman, 1991). Crystal growth can be expected to be more easily accommodated in a direction parallel to those slices than in other directions.

Omongwaite developed along bounding surfaces of gypsum crystals, subsequently covered by a later growth stage of gypsum. The nature of these surfaces ranges from curved or straight crystal faces to irregular sides of cavities within the gypsum crystals. The direction of growth of the omongwaite crystals is always towards the interior of the affected gypsum crystal. They are covered by overgrowths that generally have a high sediment content, either throughout the outer part of the gypsum crystal or within a thin band along the base of the omongwaite crystals. Within gypsum crystals in which the inclusions surround a zone with a high sediment content, with an outward orientation of the euhedral terminations, the overgrowth is a sediment-rich epitaxial infilling of a cavity.

Omongwaite formed by an interaction of gypsum with brines whose evolution was marked by an increase in salinity by evaporation and an increase in relative Na^+ and K^+ concentrations by extensive gypsum formation. Omongwaite formed at least partly in recent times, as indicated by its presence in prismatic gypsum crystals in the surface layer. Present-day brine compositions, with molar Na/K and (Na+K)/Ca ratios of about 10, therefore give an indication of the conditions that can lead to omongwaite formation.

Omongwaite has a higher solubility than gypsum and is only preserved where a gypsum

overgrowth developed shortly after its formation; observations for a crystal that is only partly covered by an overgrowth, showing only remnants of inclusions (see Fig. 4*c*), are compatible with this. The large sediment content of these overgrowths indicates that they formed by rapid crystal growth at high salinities. These observations imply that the formation of omongwaite and its preservation, by the development of the gypsum overgrowths, are related events. Formation within a short time period is also suggested by the occurrence of randomly-oriented omongwaite inclusions within the sediment-rich core of some gypsum crystals.

Conclusions

Omongwaite is a new mineral that occurs as inclusions in gypsum crystals from a dry lake basin of the southwestern Kalahari. It represents the end-member of compounds with a continuous range of compositions between itself and bassanite. The Na/K ratio is variable, determined by physicochemical and structural factors that are, as yet, not clearly understood. Omongwaite should not be expected to be extremely rare in evaporite deposits. Rather exceptional conditions might be required for its formation and preservation, but the lack of earlier reports could mainly be related to confusion with bassanite, a closely related phase.

Acknowledgements

FM is grateful to the following persons for their assistance in obtaining analytical data during various stages of this study: Stuart Kearns (University of Bristol), Alain Bernard (Université Libre de Bruxelles), Norbert Blaton (Katholieke Universiteit Leuven), Gordon Cressey and John Francis (Natural History Museum, London), Herman Goethals (Koninklijk Belgisch Instituut voor Natuur-wetenschappen, Brussels), Peter Vandenabeele (Universiteit Gent), and Renaud Vochten (Universiteit Antwerpen). Microprobe analysis was made possible by the support of the European Community Access to Research Infrastructure action of the Improving Human Potential Programme (contract HPRI-CT-1999-00008, awarded to Bernard J. Wood, EU Geochemical Facility, University of Bristol). FH acknowledges the support of the FRS-FNRS (Belgium) by granting a 'chercheur qualifié' position.

References

Autenrieth, H. (1958) Untersuchungen im Sechs-Komponenten-System K^+, Na^+, Mg^{2+}, Ca^{2+}, SO_4^{2-}, (Cl^-), H_2O mit Schlussfolgerungen für die Verarbeitung der Kalisalze. *Kali und Steinsalz*, **2**, 181–200.

Autenrieth, H. and Braune, G. (1959) Das Sechs-Komponenten-System K^+, Na^+, Mg^{2+}, Ca^{2+}, SO_4^{2-}, (Cl^-), H_2O bei 90º und seine Anwendung auf Schlammprobleme der Kalisalzverarbeitung. *Kali und Steinsalz*, **2**, 395–405.

Bellanca, A. (1942) L'aftitalite nel sistema ternario K_2SO_4-Na_2SO_4-$CaSO_4$. *Periodico di Mineralogia*, **13**, 21–86.

Bensted, J. and Prakash, S. (1968) Investigation of the calcium sulphate-water system by infrared spectroscopy. *Nature*, **219**, 60–61.

Chang, H., Huang, P.J. and Hou, S.C. (1999) Application of thermo-Raman spectroscopy to study dehydration of $CaSO_4.2H_2O$ and $CaSO_4.0.5H_2O$. *Materials Science and Physics*, **58**, 12–19.

Chio, C.H., Sharma, S.K. and Muenow, D.W. (2004) Micro-Raman studies of gypsum in the temperature range between 9 K and 373 K. *American Mineralogist*, **89**, 390–395.

Dickinson, R.G. and Dillon, R.T. (1929) The Raman spectrum of gypsum. *Proceedings of the National Academy of Sciences*, **15**, 695–699.

Du, H. (2000) Thermodynamic assessment of the K_2SO_4-Na_2SO_4-$MgSO_4$-$CaSO_4$ system. *Journal of Phase Equilibria*, **21**, 6–18.

Eipeltauer, E. (1956) Die Bedeutung kalorimetrischer Messungen für die Gipserzeugung und Gipsprüfung. *Zement-Kalk-Gips*, **9**, 501–505.

Freyer, D., Reck, G., Bremer, M. and Voigt, W. (1999) Thermal behaviour and crystal structure of sodium-containing hemihydrates of calcium sulfate. *Monatshefte für Chemie*, **130**, 1179–1193.

Freyer, D., Ziske, S. and Voigt, W. 2002. Thermoanalytische und FT-ramanspektroskopische Untersuchungen zur Bildung und Umwandlung von $CaSO_4$-Halbhydraten. *Freiberger Forschungshefte*, **E3**, 127–136.

Greenberg, J.P. and Møller, N. (1989) The prediction of mineral solubilities in natural waters: a chemical equilibrium model for the Na-K-Mg-Ca-Cl-SO_4-H_2O system to high concentration from 0 to 250ºC. *Geochimca et Cosmochimica Acta*, **53**, 2503–2518.

Gudowius, E. and Von Hodenberg, R. (1979) 'Natriumpolyhalit', eine dem Bassanit und dem γ-$CaSO_4$ verwandte Phase. *Kali und Steinsalz*, **7**, 501–504.

Harvie, C.E. and Weare, J.H. (1980) The prediction of mineral solubilities in natural waters: the Na-K-Mg-Ca-Cl-SO_4-H_2O system from zero to high concentration at 25ºC. *Geochimica et Cosmochimica Acta*, **44**,

981–997.

Hass, M. and Sutherland, G.B.B.M. (1956) The infra-red spectrum and crystal structure of gypsum. *Proceedings of the Royal Society of London*, **236**, 427–445.

Heijnen, W.M.M. and Hartman, P. (1991) Structural morphology of gypsum ($CaSO_4.2H_2O$), brushite ($CaHPO_4.2H_2O$) and pharmacolite ($CaHAsO_4.2H_2O$). *Journal of Crystal Growth*, **108**, 290–300.

Hill, A.E. and Wills, J.H. (1938) Ternary systems. XXIV. Calcium sulfate, sodium sulfate and water. *Journal of the American Chemical Society*, **60**, 1647–1655.

Kloprogge, J.T. and Frost, R.L. (2000) Raman spectroscopy at 77 K of natural gypsum $CaSO_4.2H_2O$. *Journal of Materials Science Letters*, **19**, 229–231.

Kushnir, J. (1982) The partitioning of seawater cations during the transformation of gypsum to anhydrite. *Geochimica et Cosmochimica Acta*, **46**, 433–446.

Lager, G.A., Armbruster, T., Rotella, F.J., Jorgensen, J.D. and Hinks, D.G. (1984) A crystallographic study of the low-temperature dehydration products of gypsum, $CaSO_4.2H_2O$: hemihydrate $CaSO_4.0.50H_2O$, and γ-$CaSO_4$. *American Mineralogist*, **69**, 910–919.

Lepeshkov, I.N. and Fradkina, Kh.B. (1959) Salt solubilities in the $CaSO_4$-Na_2SO_4-NaCl-H_2O system at 35º and 55º. *Russian Journal of Inorganic Chemistry*, **4**, 1297–1301.

Mees, F. (1999) Distribution patterns of gypsum and kalistrontite in a dry lake basin of the southwestern Kalahari (Omongwa pan, Namibia). *Earth Surface Processes and Landforms*, **24**, 731–744.

Pouchou, J.L and Pichoir, F. (1988) A simplified version of the 'PAP' model for matrix corrections in EPMA. Pp. 315–318 in: *Microbeam Analysis* (D.E. Newbury, editor). San Francisco Press, San Francisco, USA.

Powell, D.A. (1962) Calcium sulphate hemihydrate prepared in sodium chloride solution. *Australian Journal of Chemistry*, **15**, 868–874.

Prasad, P.S.R. (1999) Raman intensities near gypsum-bassanite transition in natural gypsum. *Journal of Raman Spectroscopy*, **30**, 693–696.

Prasad, P.S.R., Ravikumar, N., Krishnamurthy, A.S.R. and Sarma, L.P. (1998) Role of impurities in gypsum-bassanite phase transition: a comparative Raman study. *Current Science*, **75**, 1410–1414.

Prasad, P.S.R., Chaitanya, V.K., Prasad, K.S. and Rao, D.N. (2005) Direct formation of the γ-$CaSO_4$ phase in dehydration process of gypsum: in situ FTIR study. *American Mineralogist*, **90**, 672–678.

Putnis, A., Winkler, B. and Fernandez-Diaz, L. (1990) *In situ* IR spectroscopic and thermogravimetric study of the dehydration of gypsum. *Mineralogical Magazine*, **54**, 123–128.

Rassonskaya, I.S. and Semendyaeva, N.K. (1961) Phase transformations of calcium and sodium sulphates and their double salts. *Russian Journal of Inorganic Chemistry*, **6**, 891–895.

Reisdorf, K. and Abriel, W. (1987) Reactionen im System $CaSO_4$-H_2O und über Na-Polyhalite $Na_2Ca_5(SO_4)_6(H_2O)_3$. *Neues Jahrbuch für Mineralogie Abhandlungen*, **157**, 35–46.

Rogozovskaya, M.Z., Kononchuk, T.I. and Lukjanova, N.K. (1980) Phase transformations of gypsum and sodium pentasalt $5CaSO_4.Na_2SO_4.3H_2O$ in concentrated sodium chloride solutions. *Russian Journal of Inorganic Chemistry*, **25**, 608–612.

Rogozovskaya, M.Z. and Kononchuk, T.I. (1981) Crystallization of gypsum and of sodium pentasalt during desulfation of sodium chloride solutions. *Journal of Applied Chemistry of the U.S.S.R.*, **54**, 1460–1463.

Rowe, J.J., Morey, G.W. and Zen, C.S. (1972) The quinary reciprocal salt system Na,K,Mg,Ca/Cl,SO_4 – A review of the literature with new data. *U.S. Geological Survey Professional Paper*, **741**, 37 pp.

Sarma, L.P., Prasad, P.S.R. and Ravikumar, N. (1998) Raman spectroscopic study of phase transitions in natural gypsum. *Journal of Raman Spectroscopy*, **29**, 851–856.

Viljoen, J.J. and Kamupingene, T.K. (1983) *Otjiherero*. Gamsberg Publishers, Windhoek, Namibia.

Weijnen, M.P.C., van Rosmalen, G.M., Bennema, P. and Rijpkema, J.J.M. (1987) The adsorption of additives at the gypsum crystal surface: A theoretical approach. I. Determination of the interfacial bond energies. *Journal of Crystal Growth*, **82**, 509–527.